ACS APPLIED MATERIALS & INTERFACES

Research Article

www.acsami.org

Facile Preparation and Thermoelectric Properties of Bi_2Te_3 Based Alloy Nanosheet/PEDOT:PSS Composite Films

Yong Du,[†,‡] K. F. Cai,*[,†,§] Song Chen,[†] Pavel Cizek,[‡] and Tong Lin*[,‡]

[†]Functional Materials Research Laboratory, Tongji University, 4800 Caoan Road, Shanghai 201804, China

[‡]Institute for Frontier Materials, Deakin University, Geelong, VIC 3216, Australia

[§]State Key Lab of Silicon Materials, Zhejiang University, Hangzhou, 310027 Zhejiang, China

ABSTRACT: Bi_2Te_3 based alloy nanosheet (NS)/poly(3,4-ethylenedioxythiophene):poly(4-styrenesulfonate) (PEDOT:PSS) composite films were prepared separately by spin coating and drop casting techniques. The drop cast composite film containing 4.10 wt % Bi_2Te_3 based alloy NSs showed electrical conductivity as high as 1295.21 S/cm, which is higher than that (753.8 S/cm) of a dimethyl sulfoxide doped PEDOT:PSS film prepared under the same condition and that (850−1250 S/cm) of the Bi_2Te_3 based alloy bulk material. The composite film also showed a very high power factor value, ~32.26 μWm^{-1} K^{-2}. With the content of Bi_2Te_3 based alloy NSs increasing from 0 to 4.10 wt %, the electrical conductivity and Seebeck coefficient of the composite films increase simultaneously.

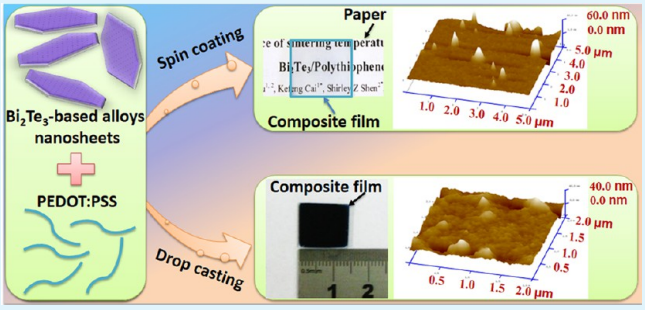

KEYWORDS: *Bi_2Te_3, poly(3,4-ethylenedioxythiophene):poly(4-styrenesulfonate), thermoelectric properties, composite films*

1. INTRODUCTION

Power generation from fossil fuels and nuclear energy is often accompanied by substantial heat losses (~60%). About 50% of the waste heat is stored in large volume fluids (temperature <250 °C) which has not yet been utilized effectively.[1] Thermoelectrics (TEs) offers a promising solution to recover low-grade waste heat into electricity. TE devices have many attractive features, such as long operating lifetime, no moving parts, no noise, easy maintenance, environmentally friendly, and highly reliable.[2,3]

The TE performance of a material is evaluated by the material's dimensionless figure of merit, $ZT = S^2\sigma T/\kappa$ (where S is the Seebeck coefficient, σ is the electrical conductivity, κ is the thermal conductivity, and T is the absolute temperature).[4] However, the above-mentioned three parameters (S, σ, and κ) are determined by the details of the electronic structure and scattering of charge carriers and thus are not independent. Therefore, it is quite difficult to get high ZT value (say ZT > 1.5) materials. Theoretical calculations and experiments have both shown that low-dimensional TE materials have enhanced ZT values, due to the quantum size effect and enhanced interface scattering of phonons.[2,5−9]

Most of the previous efforts in the TE community have been focused on inorganic TE materials. Bi_2Te_3 based alloy is reported to be the best TE material system at room temperature (RT). Much attention has been paid to improving the TE properties of Bi_2Te_3 based alloys.[9−12] Those having high TE performances are mainly achieved by reducing thermal conductivity resulting from nanostructures in the materials. However, expensive raw material and high processing cost, heavy metal pollution, and poor processability have limited their broad applications.[13−16]

Although conducting polymers usually have a power factor (PF, $S^2\sigma$) ranging from 10^{-6} to 10^{-10} $W{\cdot}m^{-1}{\cdot}K^{-2}$, which is 3 orders of magnitude lower than that of the state-of-the-art inorganic TE materials,[17−20] they possess unique features such as low thermal conductivity, low density, low cost, easy synthesis, and relatively facile to be processed into versatile forms.[13] More and more attention has recently been paid toward the TE properties of conducting polymers and inorganic TE nanostructure/conducting polymer nanocomposites, and much progress has been made.[1,21−30] For example, a tosylate doped poly(3,4-ethylenedioxythiophene) (PEDOT) film with ZT = 0.25 at RT[31] and a poly(styrenesulfonate) (PSS) doped PEDOT film with ZT = 0.42 at RT[32] were successively reported. A nanocomposite consisting of inorganic TE nanostructures and a conducting polymer is expected to take advantage of both components to lower cost but improve TE performance. However, until now, inorganic nanostructure/conductive polymer nanocomposites with effectively enhanced ZT values at RT have still not been developed (the highest ZT value reported for inorganic nanostructure/polymer nanocomposites is the Te/PEDOT:PSS film with ZT ~ 0.10 at RT[29]). There are three main reasons for this result: 1) Generally, conducting polymers or inorganic TE nanostructure/polymer nanocomposites, like inorganic TE materials, and

Received: January 20, 2014
Accepted: March 25, 2014
Published: March 25, 2014

   dx.doi.org/10.1021/am5002772 | ACS Appl. Mater. Interfaces 2014, 6, 5735−5743

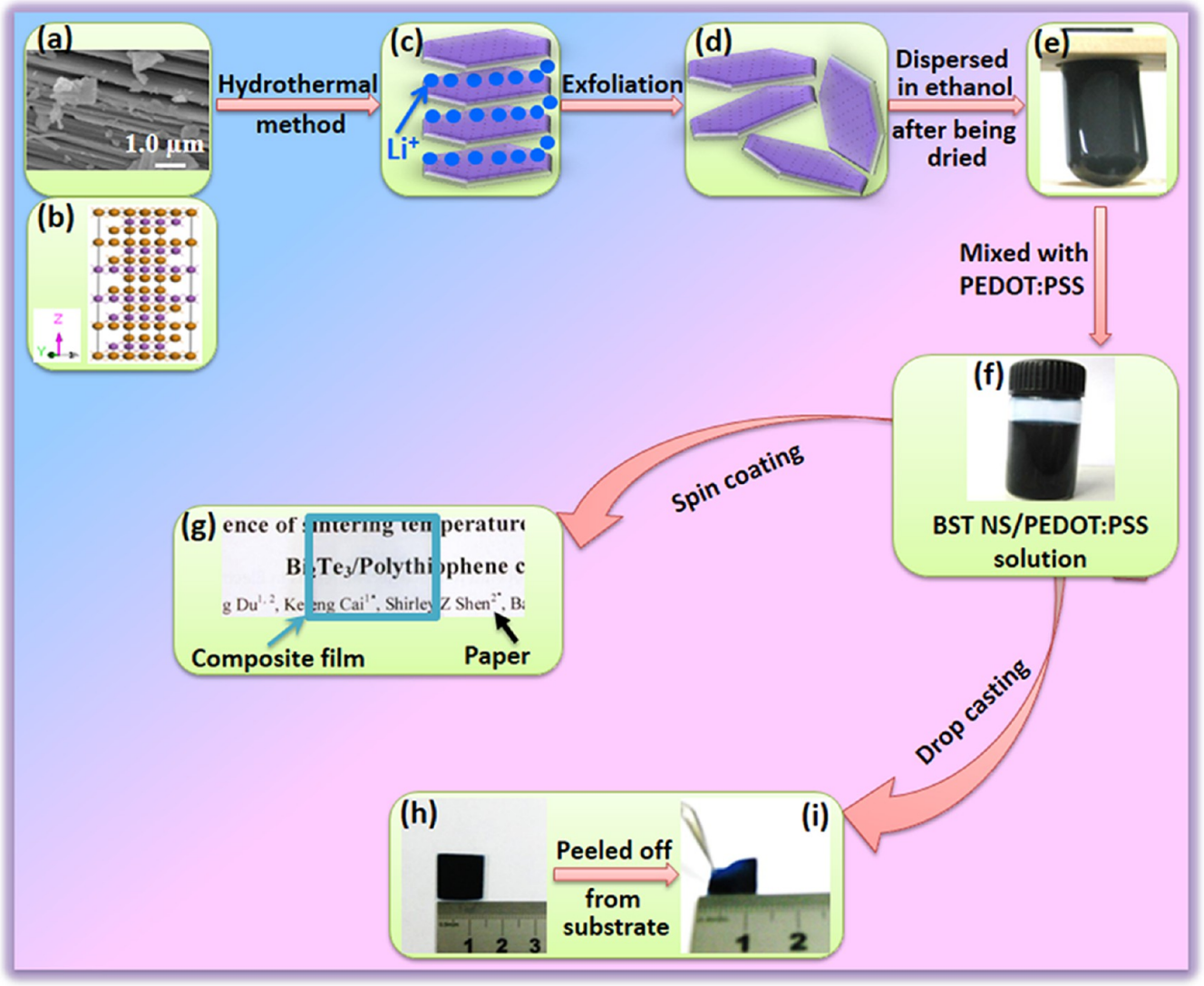

Figure 1. Illustration of the process for preparation of BST NS/PEDOT:PSS films. (a) typical FESEM image of the BST ingot after grinding, (b) crystal structure of Bi_2Te_3 (• (yellow): Te, • (purple): Bi), (c) Li-intercalated units after hydrothermal process, (d) BST NSs after being exfoliated, (e) BATA NSs dispersed in ethanol, (f) BST NS/PEDOT:PSS solution, (g) spin coated BST NS/PEDOT:PSS film on a glass substrate (marked by a blackish green square), (h) drop cast BST NS/PEDOT:PSS film on a glass substrate, and (i) drop cast BST NS/PEDOT:PSS film after being peeled off from the glass substrate.

their σ, κ, and S are interdependent.[8,15] Changing one parameter alters the others making the optimization of these contradictory properties extremely difficult.[33] Previously studies on stretched polyaniline (PANI) films,[34] β-naphthalene sulfonic acid doped PANI nanotubes,[35] organo-soluble PANI doped with HCl,[36] and tetrafluorotetracyanoquinodimethane doped poly(3-hexylthiophene) film[37] have indicated that σ and S increased simultaneously because of the improved molecular ordering of polymer chains and increased charge carrier mobility. However, it is still difficult to increase the σ and S simultaneously in inorganic nanostructure/conductive polymer nanocomposites. 2) The research on the TE properties of inorganic TE nanostructure/polymer nanocomposites is mainly focused on choosing suitable methods for synthesis of the composites and varying the content of inorganic TE nanostructures to optimize the TE properties, whereas the TE properties of polymer matrix are not optimized. 3) The present techniques for preparation of inorganic nanostructure/conductive polymer nanocomposites, such as physical mixing,[38,39] and solution mixing,[40] *in situ* oxidative polymerization[19,41] still remain difficult in dispersing inorganic TE nanostructures in polymer matrix. Poor wettability between polymer and inorganic TE nanostructures and easy oxidation of inorganic TE nanostructures during the processing have prevented inorganic TE nanostructures from effective dispersion in a polymer matrix.[38−40] *In situ* synthesis technique[29] can avoid the oxidation of the nanostructures; however, this technique is not universal.

Most recently, Song et al.[42] prepared Bi_2Te_3/PEDOT:PSS TE composite films by a physical mixing method with different contents of the Bi_2Te_3 particle, and the highest power factor of 9.9 $\mu Wm^{-1} K^{-2}$ was reported for the composite film with 10 wt % Bi_2Te_3. Despite the method used being simple, the power factor is relatively low. One of the reasons for the low power factor could be that the Bi_2Te_3 particles (325 mesh) used are in micrometer sized, which cannot be homogeneously dispersed in the PEDOT:PSS matrix. Interestingly, Ren et al.[43] reported a convenient hydrothermal intercalation/exfoliation method for

the manufacturing of 3−4 nm thick Bi_2Te_3 nanosheets (NSs). The NSs are so thin that they can be effectively dispersed in ethanol, and PEDOT:PSS is water-soluble; this means that the NSs and PEDOT:PSS can be well dispersed with each other in aqueous solution. PEDOT:PSS is the best conducting polymer,[44,45] and it has shown very promising TE properties after optimization.[31] In this work, we first prepared the Bi_2Te_3 based alloy, $Bi_{0.5}Sb_{1.5}Te_3$ (BST, which is the best composition for p-type Bi_2Te_3 based alloys), NSs by the method described in ref 43, and then prepared BST NS/PEDOT:PSS composite films by two methods: drop casting and spin coating, and characterized the microstructure and TE properties of the films.

2. EXPERIMENTAL SECTION

2.1. Materials. P-type BST ingot (with composition of $Bi_{0.5}Sb_{1.5}Te_3$ determined by energy-dispersive spectrometry (EDS)) was obtained from Thermonamic Electronics (Jiangxi) Corp., Ltd. (σ: 850−1250 S/cm, S: 190−230 μV/K, at RT). Lithium hydroxide, dimethyl sulfoxide (DMSO), acetone, and porous polyvinylidene fluoride (PVDF) (0.45 μm nominal pore size) membranes were purchased from Sinopharm Chemical Reagent Co., Ltd. PEDOT:PSS (Clevios PH 1000) was purchased from H. C. Stark, Inc. All the materials were used as received.

2.2. Exfoliation of BST. In a typical procedure for exfoliation of BST,[43] BST ingot was ground in an agate mortar for 90 min to get fine powder. The powder was then placed into a 100 mL Teflon-lined autoclave filled with an ethylene glycol solution of lithium hydroxide (8 g/L). The autoclave was performed in an oven at 200 °C for 24 h to intercalate lithium ions (Li^+) into BST. The Li^+ intercalated suspension was collected by filtration and rinsed with acetone to eliminate excess lithium hydroxide and ethylene glycol. Upon adding the lithiated powder to deionized water, BST was readily exfoliated into a colloidal suspension. BST NS membranes were obtained by filtering the final BST with a porous PVDF membrane. After drying in vacuum at 60 °C for 12 h, the samples were ready for characterization.

2.3. Preparation of BST NS/PEDOT:PSS Films. Glass substrates (2 cm × 2 cm) were ultrasonicated in acetone for 15 min and oxidized in Piranha solution [V(98% H_2SO_4): V(30% H_2O_2) = 7:3] for 1 h before rinsing with distilled water. An appropriate amount of DMSO was mixed with the PEDOT/PSS solution to form 10 wt % of DMSO/PEDOT:PSS mixture. The mixture was sonicated for 1 h at RT and then filtered through a 0.45 μm PVDF membrane to remove any traces of undissolved aggregates. An appropriate amount of BST NSs (dispersed in ethanol) was added to the above mixture and sonicated for 1 h to produce solutions containing 2.09, 4.10, 7.87, or 9.65 wt % BST NSs. BST NS/PEDOT:PSS composite films were prepared by drop casting or spin coating (1000 rpm for 60 s followed by 2000 rpm for 60 s) the mixed solutions on glass substrates (2 cm × 2 cm) and then dried in vacuum at 60 °C for 1 h. This process is schematically depicted in Figure 1. For comparison, the pure PEDOT:PSS film was also prepared using the same procedure.

2.4. Characterizations. The morphology of the samples was examined by field emission scanning electron microscopy (FESEM), transmission electron microscopy (TEM, Philips TECNAI-20), and atomic force microscopy (AFM). AFM was performed with Digital Instruments Nanoscope III operating in tapping mode. The FESEM samples were coated with gold before observation. The thickness of the BST/PEDOT:PSS composite films was determined by FESEM and XP-plus stylus profilometer (AMBIOS XP-2000). The Hall effect was measured using an HMS-3000 (Ecopia) system with a magnetic field of 0.55 T at RT. In-plane electrical conductivity and Seebeck coefficient of the composite films were measured at RT. The electrical conductivity was measured using a steady-state four-probe technique with a square wave current (~10 mA in amplitude). The Seebeck coefficient was obtained from the slope of the linear relationship between thermal electromotive force and temperature difference (~10 K) of two points on each film.

3. RESULTS AND DISCUSSION

Figures 2 (a)−(c) show the TEM images of the as-prepared BST NSs. BST NSs looked very thin with smooth surface. The

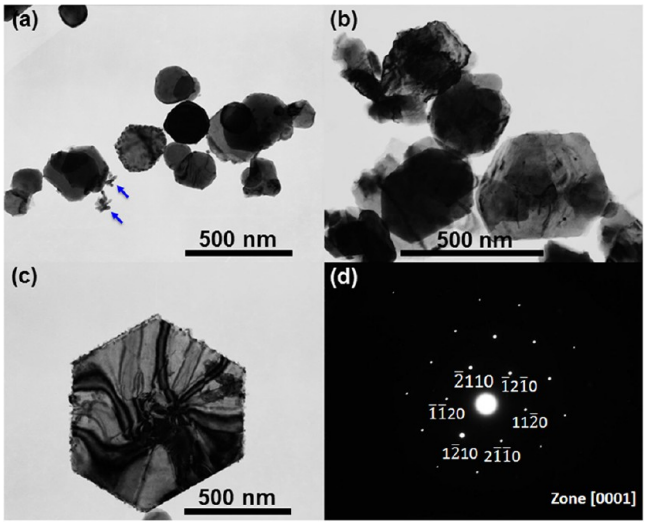

Figure 2. (a), (b), and (c) TEM images of the P-type BST NSs and (d) the selected area electron diffraction pattern corresponding to the BST NS in (c).

edge length of the hexagonal NSs varied from ~125 to 800 nm (see Figures 2 (a)−(c)). Besides the BST NSs, a small amount of BST nanorods and approximately spherical nanoparticles were also observed, as indicated by arrows in Figure 2 (a). Figure 2 (d) shows a hexagonal electron diffraction pattern of the BST NS as shown in Figure 2 (c), indicating the single crystalline nature of the BST NSs and that the growth direction of the BST NSs is along the basal plane of the Bi_2Te_3 crystal structure (see Figure 1 (b)), which is the direction with the best TE properties of Bi_2Te_3.[46] This result is in good accordance with the result reported in ref 43.

Figures 3 (a)−(d) present the FESEM images of the drop cast BST NS/PEDOT:PSS composite films. The film surface became rougher with the BST NS content increasing from 2.09 to 9.65 wt %. The inset in Figure 3 (a) shows the FESEM image of the fracture surface perpendicular to the composite film (2.09 wt % BST NSs). The film thickness measured based on the inset image was 4.53 μm. These films showed excellent flexibility (see Figure 1 (i)), which can be rolled up, bent, or twisted and even folded easily without cracking, which is superior to conventional fragile TE films.

Figures 3 (e) and (f) present the FESEM images of the 9.65 wt % BST NS/PEDOT:PSS composite films prepared by spin coating. BST NSs were homogeneously dispersed in the PEDOT:PSS matrix. The composite films are highly transparent to visible light (see Figure 1 (g)).

Some bulges were observed on the film surface, which were attributed to the aggregation of BST NSs within the film. Compared with the drop cast films, the spin coated films had rougher surface. This is mainly because the films are much thinner (thickness 80−120 nm) than the drop cast ones (thickness 2.5−5.5 μm), resulting from different film forming methods. The rodlike and spherical BST particles within the films have a stronger effect on their surface roughness than the BST NSs.

dx.doi.org/10.1021/am5002772 | ACS Appl. Mater. Interfaces 2014, 6, 5735−5743

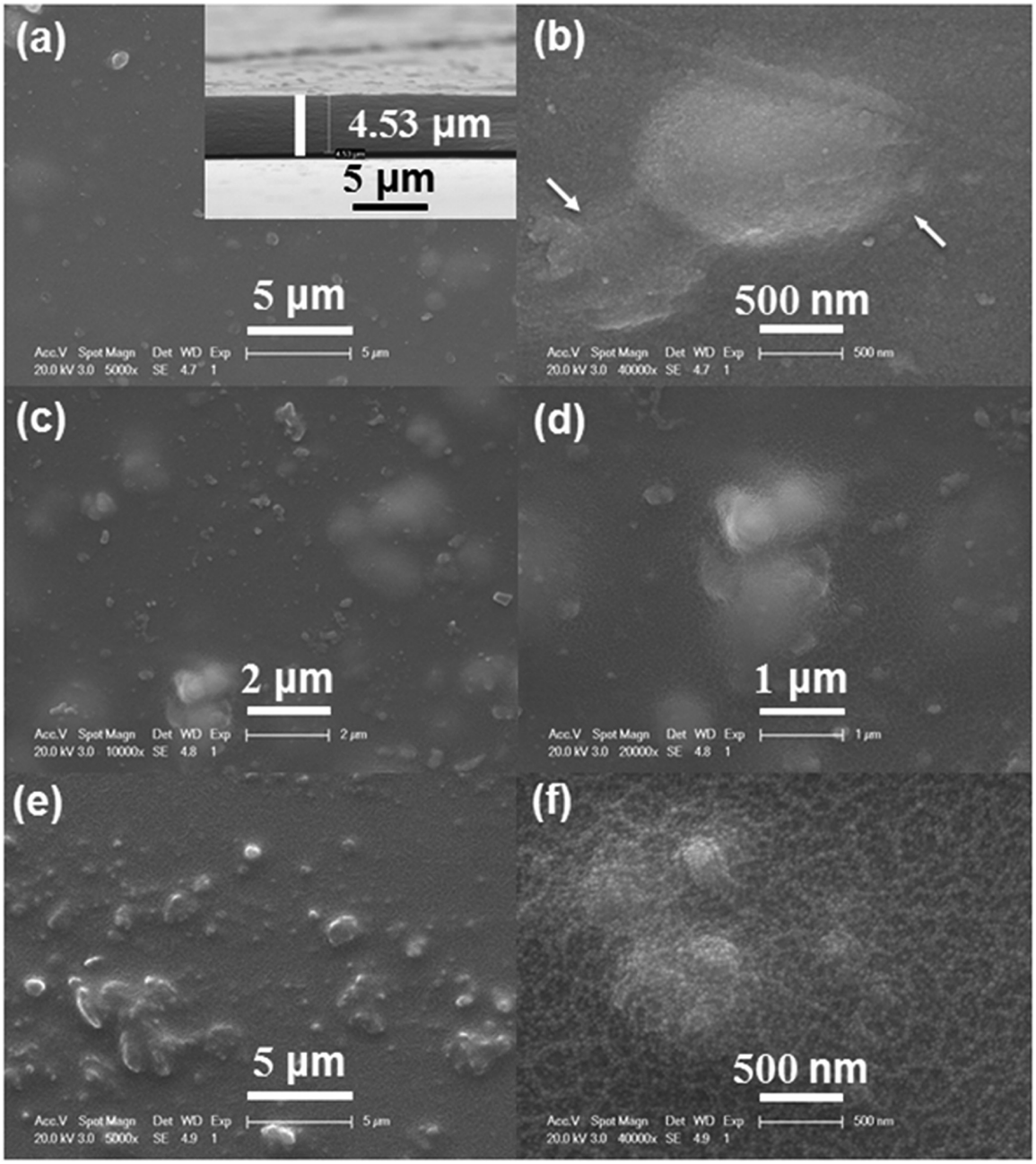

Figure 3. FESEM images of the drop cast BST NS/PEDOT:PSS composite films containing (a) and (b) 2.09 wt %, (c) and (d) 9.65 wt % BST NSs, and (e) and (f) spin coated 9.65 wt % BST NS/PEDOT:PSS composite films. The inset in (a) shows the fracture surface of the composite film shown in (a).

Figure 4 presents the topographic AFM images of the drop cast BST NS/PEDOT:PSS composite films. The drop cast films with a low BST NS content (e.g., 2.09 wt %) look very smooth for the most part (see Figures 4 (a) and (b)), and in this case, the BST NSs can be seen clearly in the PEDOT:PSS matrix (see Figures 4 (d) and (e)). As the content of BST NSs increased from 2.09 to 9.65 wt %, the surface roughness increased. Based on AFM imaging, the root-mean-square roughness (RMS) was estimated. For the drop cast composite films, the RMS increased from 2.03 to 4.97 nm, as the BST NSs content in the film increased from 2.09 to 9.65 wt %. In comparison, the RMS for the spin coated film containing 9.65 wt % BST NSs was 7.10 nm. These results are in good agreement with the corresponding three-dimensional images (see Figures 4 (b), (e), (h), and (k)), height profiles (see Figures 4 (c), (f), (i) and (l)), and FESEM observation (see Figure 3).

The room-temperature electrical conductivity, Seebeck coefficient, and calculated power factor of the composite films are presented in Figure 5. As the content of BST NSs increased from 0 to 9.65 wt %, the electrical conductivity of the spin coated composite films decreased, while the drop cast composite films increased first and then slightly decreased.

The electrical conductivity of the spin coated composite films was much lower than that of the drop cast composite films. This mainly should be because the former is in nanometer size and its surface is rougher, which makes a difference.

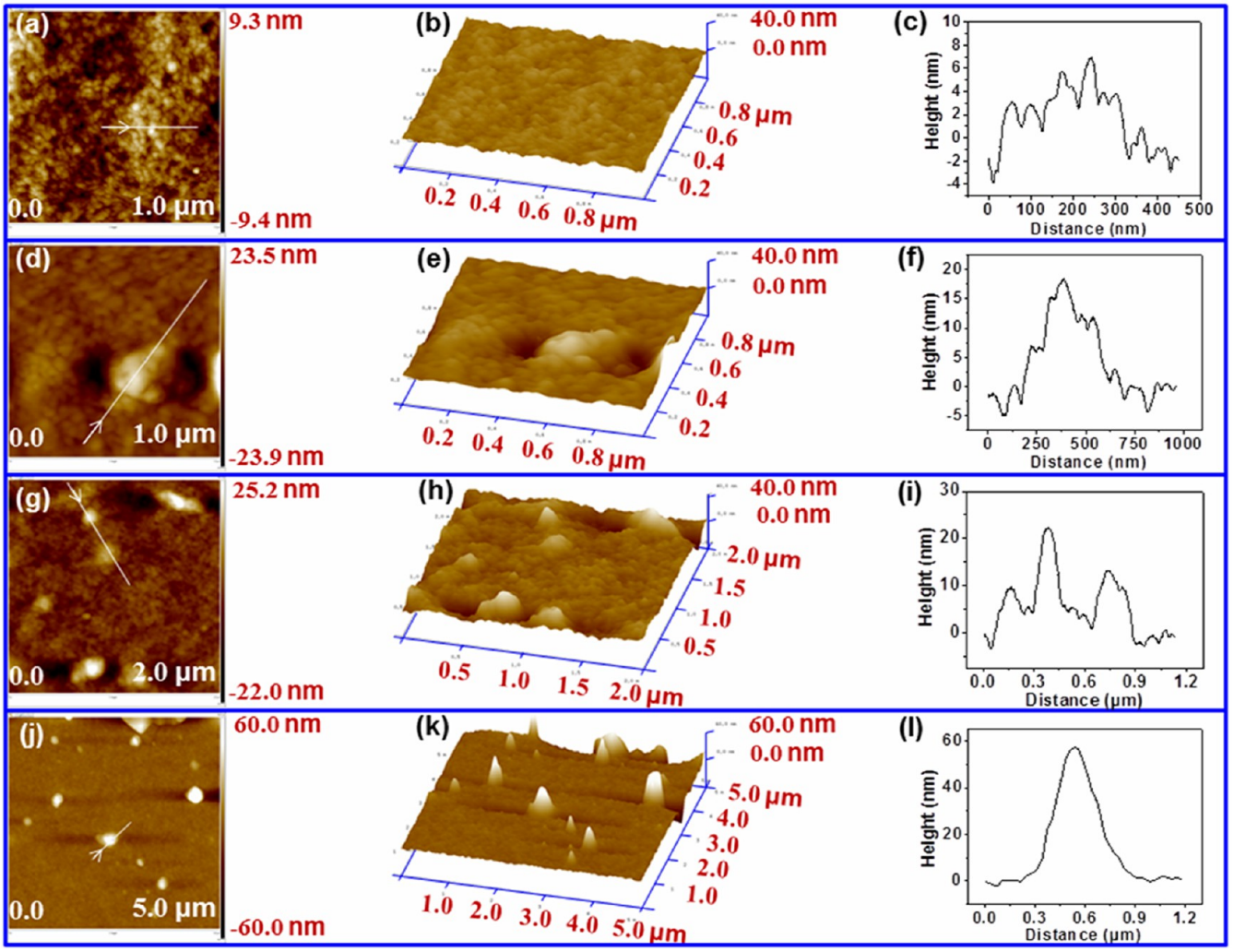

Figure 4. Topographic AFM images of the drop cast BST NS/PEDOT:PSS composite films containing 2.09 wt % (a), (d), and 9.65 wt % (g) BST NSs and (j) spin coated 9.65 wt % BST NS/PEDOT:PSS composite films. (b), (e), (h), and (k) are three-dimensional images corresponding to (a), (d), (g), and (j), respectively. (c), (f), (i), and (l) are height profiles corresponding to (a), (d), (g), and (j), respectively.

When the BST NS content was 4.10 wt %, the drop cast composite film had the highest electrical conductivity (1295.2 S/cm) among all the samples (see Figures 5 (a) and (b)). This value is higher than that of the DMSO doped PEDOT:PSS film prepared under the same condition (753.8 S/cm) and the BST bulk raw material (850−1250 S/cm at RT described by the manufacturer). Such a high electrical conductivity was attributed to the following two reasons: 1) BST NSs grow along the basal plane of the crystal structure. The anisotropic characteristics and dispersion in parallel to the in-plane direction of the film considerably increased electrical conductivity;[47] 2) BST has the same crystal structure as Bi_2Te_3 (the Sb atom in BST locates at the Bi-site of Bi_2Te_3 crystal structure). Bi_2Te_3 is with a rhombohedral-hexagonal symmetry (space group $R3m$ (D^5_{3d})) and demonstrates a layered structure with two types of tellurium atoms ($Te^{(1)}$ and $Te^{(2)}$).[48,49] The layers are stacked along the c axis in the following sequence (see Figure 1(b)):

$$\cdots Te^{(1)}-Bi-Te^{(2)}-Bi-Te^{(1)}\cdots Te^{(1)}-Bi-Te^{(2)}-Bi-Te^{(1)}\cdots$$

The Bi and Te layers are held together by strong covalent bonds, whereas the adjacent Te layers exhibit van der Waals bonding.[48] The combined interaction of attraction between the van der Waals bond at the $Te^{(1)}$ site and the π-system of the PEDOT:PSS chain made the nanocomposites with the ordered molecular arrangement, leading to an increase in carrier mobility and the electrical conductivity.[49] This conductivity value is also higher than that of the reported PEDOT:PSS/Te composite film (~19.3 S/cm),[29] PEDOT:PSS (Clevios PH1000)/Bi_2Te_3 composite (55−250 S/cm),[50] and PEDOT:PSS/single walled carbon nanotube composite (280−400 S/cm).[51]

The Seebeck coefficient of the BST NS/PEDOT:PSS composite films is shown in Figures 5 (a) and (b). As the content of BST NSs increased from 0 to 9.65 wt %, the Seebeck coefficient increased for both BST NS/PEDOT:PSS composite films. Compared with the drop cast ones, the spin coated composite films showed an obviously higher Seebeck coefficient. This can be attributed to two reasons: 1) the higher surface roughness of the spin coated films lead to strong carrier scattering; 2) the quantum-confinement effect of thin film prepared by the spin coating method.[52]

For the spin coated composite film containing 9.65 wt % BST NSs, the Seebeck coefficient was the highest (47.5 μV/K) among all composite films studied (see Figures 5 (a) and (b)). This value is also higher than those of the DMSO doped

dx.doi.org/10.1021/am5002772 | ACS Appl. Mater. Interfaces 2014, 6, 5735−5743

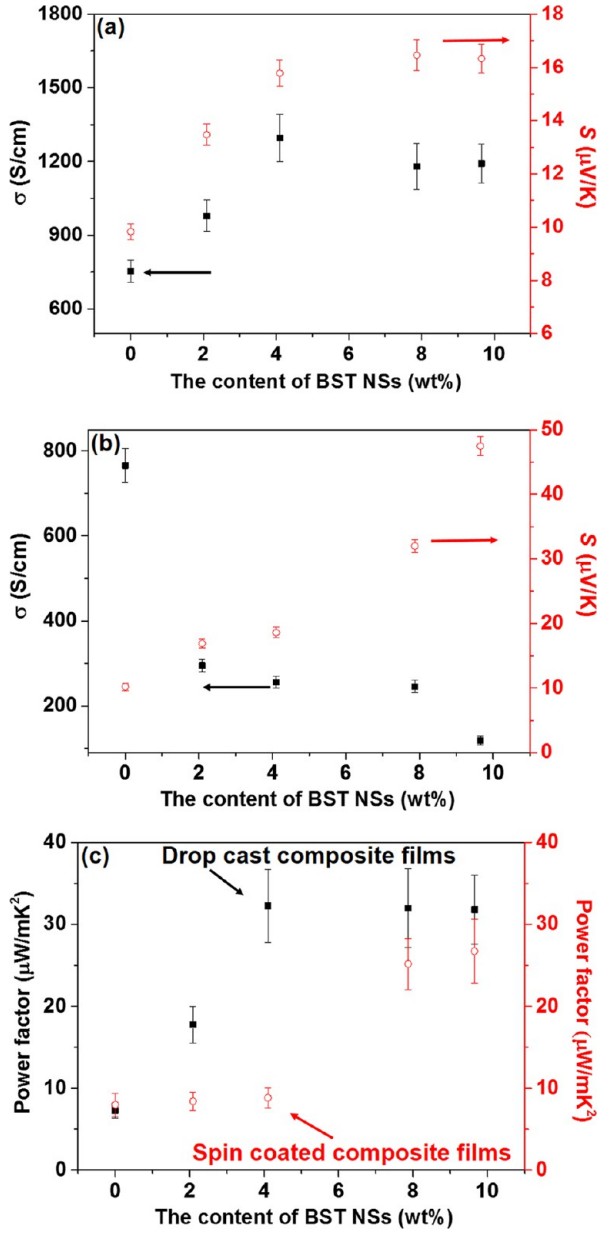

Figure 5. Electrical conductivity and Seebeck coefficient of the drop cast films (a) and the spin coated films (b) as a function of the BST NS content in the composite films, respectively. (c) Power factor calculated for the drop cast and the spin coated films as a function of the BST NS content in the composite films.

PEDOT:PSS film (10.2 μV/K) prepared under the same condition and reported PEDOT:PSS/single walled carbon nanotube composite film (~21 μV/K)[51] but lower than that of the Bi_2Te_3 bulk materials (190–230 μV/K described by the manufacturer) and that of the PEDOT:PSS/Bi_2Te_3 (~150 μV/K) composite with 90% volume fraction of p-type Bi_2Te_3,[50] mainly because of too low content of BST NSs in our film.

Figure 5 (c) shows the power factor of the composite films. With increasing the content of BST NSs, the power factor for the spin coated films increased dramatically. This was mainly because of the considerably increased Seebeck coefficient. While the power factor of the drop cast composite films first increased sharply with increasing the BST NS content from 0 to 4.10 wt %, then it almost remained unchanged with the NS content, presumably because of the sharp increase and then decrease in the electrical conductivity and gradual increase in the Seebeck coefficient of the composite films. The highest power factor value (32.26 $\mu Wm^{-1} K^{-2}$) was obtained on the drop cast composite film containing 4.10 wt % BST NSs. This value is much higher than that of the DMSO doped PEDOT:PSS film (7.28 $\mu Wm^{-1} K^{-2}$) prepared under the same condition.

Seebeck coefficient reflects intrinsic electron transport. Generally, the inverse relationship to the gap between narrow transport level (E_T) and Fermi level (E_F) results in a proportional increase of the electrical conductivity with carrier concentration. However, Seebeck coefficient for conventional semiconductors or metals decreases logarithmically with the carrier concentration.[53] In this way, the electrical conductivity and Seebeck coefficient of a material are seldom increased simultaneously. Here, the increase of both electrical conductivity and Seebeck coefficient with increasing the BST NS content from 0 to 4.10 wt %, for the drop cast composite films indicates the uniqueness of the organic–inorganic composite. It also suggests that the conduction follows a mechanism different to the band theory or the electron–phonon scattering which is used to explain conventional materials.[54]

To the best of our knowledge, it is the first time such a phenomenon is observed in the Bi–Te based alloy nanoparticle/polymer composites, although previous studies on stretched polyaniline (PANI) films,[34] β-naphthalene sulfonic acid doped PANI nanotubes,[35] organosoluble PANI doped with HCl,[36] and tetrafluorotetracyanoquinodimethane doped poly(3-hexylthiophene) film[37] have also reported the simultaneous increase in the electrical conductivity and Seebeck coefficient, which was explained that the order of polymer chains improved and hence increased the carrier mobility.

To explain the above interesting result, the Hall effect was measured. As shown in Figure 6, with increasing the content of BST NSs from 0 to 4.10 wt %, the carrier concentration decreases, while the carrier mobility increases significantly. However, the decreasing rate of the carrier concentration was lower than the increasing rate of the carrier mobility. It is known that the electrical conductivity (σ) is described as

$$\sigma = ne\mu_{(\varepsilon)} \quad (1)$$

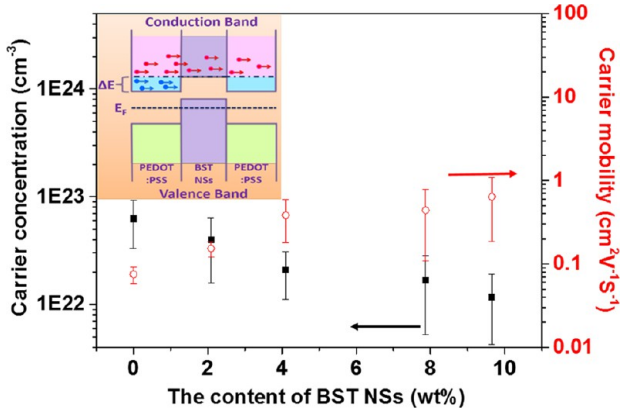

Figure 6. Carrier concentration and mobility as a function of the content of BST NSs of the drop cast BST NS/PEDOT:PSS composite films. The inset shows the illustration of the energy filtering effect in the composite films.

dx.doi.org/10.1021/am5002772 | ACS Appl. Mater. Interfaces 2014, 6, 5735–5743

where n is carrier concentration, e is the charge, and $\mu_{(e)}$ is the carrier mobility. It is easy to understand that the electrical conductivity increases when the content of BST NSs increasing from 0 to 4.10 wt %.

Seebeck coefficient is inversely proportional to the carrier concentration. As the content of BST NSs increased from 0 to 4.10 wt %, the carrier concentration decreased while the carrier mobility increased, mainly because the increase Bi_2Te_3 NS/PEDOT:PSS interfaces in the composites and nanometer-sized barriers exist on the interfaces, which may prevent low energy carriers from transmission (this effect is called "energy filtering",[55] see the inset in Figure 6). This results in an increase of the Seebeck coefficient because the value of the Seebeck coefficient is related to the thermal energy of the carriers.[55]

As the content of BST NS increases further (>4.10%), the electrical conductivity of the drop cast composite films slightly decreases, while the Seebeck coefficient slightly increases, mainly because of the shape and orientation of the BST NSs in the composite films, as well as the increase of surface roughness of the films, which leads to strong carrier scattering.

The thermal conductivities of the PEDOT:PSS and PEDOT:PSS-inorganic TE nanocomposites reported in the literature are presented in Table 1. Typically, PEDOT:PSS has much lower thermal conductivity than BST materials (the κ of single crystalline Bi_2Te_3 is ~2.8 Wm^{-1} K^{-1} at RT[56]). Surprisingly, the κ of PEDOT:PSS/Bi_2Te_3 reported in ref 42 was only 0.07 ± 0.02 W/m/K, which is much lower than that of Bi_2Te_3. Herein, as the BST NSs are imbedded in the PEDOT:PSS matrix, the thermal conductivity of the composite films should not be higher than that of the pure PEDOT:PSS due to the phonon scattering effect of the BST NSs. If the thermal conductivity of 0.2 W/m·K was taken to calculate the ZT value of the composite films, the ZT value was ~0.05 at RT for the drop cast 4.10 wt % BST NS/PEDOT:PSS composite film, which is much higher than that of the spin coated 4.10 wt % BST NS/PEDOT:PSS film (~0.01 at RT). This suggests that the manufacturing processing for the composite films has a significant influence on TE properties, and a good alternative to improve TE properties is to enhance both electrical conductivity and the Seebeck coefficient by enhancing the size-dependent energy-filtering effect and to increase the carrier mobility.

Table 1. Thermal Conductivity of PEDOT:PSS, PEDOT:Tosylate, and PEDOT:PSS-Inorganic TE Composites

year and authors	materials	κ (W/m·K)	direction
2008 Jiang et al.[57]	PEDOT:PSS pellets	0.17	
2010 See et al.[29]	PEDOT:PSS films	0.24−0.29	through-plane
	PEDOT:PSS/Te films	0.22−0.30	through-plane
2010 Scholdt et al.[58]	PEDOT:PSS films	0.32−0.34	
2010 Kim et al.[51]	PEDOT:PSS/CNT films	0.26−0.38	through-plane
2011 Bubnova et al.[31]	PEDOT:tosylate films	0.33 ± 0.1	through-plane
	PEDOT:tosylate films	0.37 ± 0.07	in-plane
2011 Yu et al.[59]	PEDOT:PSS/CNT (60 wt % CNT)	0.2−0.4	through-plane
2013 Kim et al.[32]	PEDOT:PSS films	0.22−0.3	through-plane
2013 Coates et al.[60]	PEDOT:PSS films	0.36	through-plane
	PEDOT:PSS/Te films	0.06−0.38	through-plane
2013 Song et al.[42]	PEDOT:PSS/Bi_2Te_3 films (10 wt % Bi_2Te_3)	0.07 ± 0.02	through-plane

4. CONCLUSIONS

BST NS/PEDOT:PSS nanocomposite films have been prepared by spin coating and drop casting techniques. As the content of BST NSs increases from 0 to 4.10 wt %, the electrical conductivity and the Seebeck coefficient increase simultaneously for the drop cast films. The drop cast composite film with 4.1 wt % BST NSs has the highest electrical conductivity (1295.21 S/cm) among all the composite films studied. The conductivity value is even higher than the DMSO doped PEDOT:PSS film prepared under the same condition (753.8 S/cm) and the raw BST bulk materials (850−1250 S/cm). The drop cast 4.1 wt % BST NSs composite film shows a power factor value as high as ~32.26 μWm^{-1} K^{-2}. The preparation technique and surface roughness for the films have much effect on the thermoelectric properties. This method has potential for use in other inorganic nanomaterial/polymer composite systems.

AUTHOR INFORMATION

Corresponding Authors

*Phone/Fax: +86-21-69584723. E-mail: kfcai@tongji.edu.cn (K.F.C.).

*Phone: +61 3 52271245. E-mail: tong.lin@deakin.edu.au (T.L.).

Notes

The authors declare no competing financial interest.

ACKNOWLEDGMENTS

This work was supported by the 973 Project under Grant no. 2013CB632500, National Natural Science Foundation of China (51271133), the Doctoral Program of Higher Education of China, the foundations of State Key Lab of Advanced Technology for Materials Synthesis and Processing (Wuhan University of Technology), and the State Key Lab of Silicon Materials (Zhejiang University). An Alfred Deakin postdoctoral fellowship awarded by Deakin University to the first author is acknowledged.

REFERENCES

(1) Bubnova, O.; Crispin, X. Towards Polymer-Based Organic Thermoelectric Generators. *Energy Environ. Sci.* **2012**, *5*, 9345−9362.

(2) Harman, T. C.; Taylor, P. J.; Walsh, M. P.; LaForge, B. E. Quantum Dot Superlattice Thermoelectric Materials and Devices. *Science* **2002**, *297*, 2229−2232.

(3) Heremans, J. P.; Jovovic, V.; Toberer, E. S.; Saramat, A.; Kurosaki, K.; Charoenphakdee, A.; Yamanaka, S.; Snyder, G. J. Enhancement of Thermoelectric Efficiency in PbTe by Distortion of the Electronic Density of States. *Science* **2008**, *321*, 554−557.

(4) Hsu, K. F.; Loo, S.; Guo, F.; Chen, W.; Dyck, J. S.; Uher, C.; Hogan, T.; Polychroniadis, E. K.; Kanatzidis, M. G. Cubic $AgPb_mSbTe_{2+m}$: Bulk Thermoelectric Materials with High Figure of Merit. *Science* **2004**, *303*, 818−821.

(5) Boukai, A. I.; Bunimovich, Y.; Tahir-Kheli, J.; Yu, J. K.; Goddard, W. A., III; Heath, J. R. Silicon Nanowires as Efficient Thermoelectric Materials. *Nature* **2008**, *451*, 168−171.

(6) Hicks, L. D.; Dresselhaus, M. S. Effect of Quantum-Well Structures on the Thermoelectric Figure of Merit. *Phys. Rev. B.* **1993**, *47*, 12727−12731.
(7) Hicks, L. D.; Harman, T. C.; Sun, X.; Dresselhaus, M. S. Experimental Study of the Effect of Quantum-Well Structures on the Thermoelectric Figure of Merit. *Phys. Rev. B* **1996**, *53*, 10493−10496.
(8) Hochbaum, A. I.; Chen, R. K.; Delgado, R. D.; Liang, W. J.; Garnett, E. C.; Najarian, M.; Majumdar, A.; Yang, P. D. Enhanced Thermoelectric Performance of Rough Silicon Nanowires. *Nature* **2008**, *451*, 163−165.
(9) Venkatasubramanian, R.; Siivola, E.; Colpitts, T.; O'Quinn, B. Thin-Film Thermoelectric Devices with High Room-Temperature Figures of Merit. *Nature* **2001**, *413*, 597−602.
(10) Cao, Y. Q.; Zhao, X. B.; Zhu, T. J.; Zhang, X. B.; Tu, J. P. Syntheses and Thermoelectric Properties of Bi_2Te_3/Sb_2Te_3 Bulk Nanocomposites with Laminated Nanostructure. *Appl. Phys. Lett.* **2008**, *92*, 143106.
(11) Xie, W. J.; Tang, X. F.; Yan, Y. G.; Zhang, Q. J.; Tritt, T. M. Unique Nanostructures and Enhanced Thermoelectric Performance of Melt-Spun BiSbTe Alloys. *Appl. Phys. Lett.* **2009**, *94*, 102111.
(12) Poudel, B.; Hao, Q.; Ma, Y.; Lan, Y. C.; Minnich, A.; Yu, B.; Yan, X.; Wang, D. Z.; Muto, A.; Vashaee, D.; Chen, X. Y.; Liu, J. M.; Dresselhaus, M. S.; Chen, G.; Ren, Z. F. High-Thermoelectric Performance of Nanostructured Bismuth Antimony Telluride Bulk Alloys. *Science* **2008**, *320*, 634−638.
(13) Yao, Q.; Chen, L. D.; Zhang, W. Q.; Liufu, S. C.; Chen, X. H. Enhanced Thermoelectric Performance of Single-Walled Carbon Nanotubes/Polyaniline Hybrid Nanocomposites. *ACS Nano* **2010**, *4*, 2445−2451.
(14) Toshima, N. Conductive Polymers as a New Type of Thermoelectric Material. *Macromol. Symp.* **2002**, *186*, 81−86.
(15) DiSalvo, F. J. Thermoelectric Cooling and Power Generation. *Science* **1999**, *285*, 703−706.
(16) Li, J. J.; Tang, X. F.; Li, H.; Yan, Y. G.; Zhang, Q. J. Synthesis and Thermoelectric Properties of Hydrochloric Acid-Doped Polyaniline. *Synth. Met.* **2010**, *160*, 1153−1158.
(17) Du, Y.; Shen, S. Z.; Cai, K. F.; Casey, P. S. Research Progress on Polymer−Inorganic Thermoelectric Nanocomposite Materials. *Prog. Polym. Sci.* **2012**, *37*, 820−841.
(18) Levesque, I.; Bertrand, P. O.; Blouin, N.; Leclerc, M.; Zecchin, S.; Zotti, G.; Ratcliffe, C. I.; Klug, D. D.; Gao, X.; Gao, F. M.; Tse, J. S. Synthesis and Thermoelectric Properties of Polycarbazole, Polyindolocarbazole, and Polydiindolocarbazole Derivatives. *Chem. Mater.* **2007**, *19*, 2128−2138.
(19) Liu, H.; Wang, J. Y.; Hu, X. B.; Boughton, R. I.; Zhao, S. R.; Li, Q.; Jiang, M. H. Structure and Electronic Transport Properties of Polyaniline/$NaFe_4P_{12}$ Composite. *Chem. Phys. Lett.* **2002**, *352*, 185−190.
(20) Levesque, I.; Gao, X.; Klug, D. D.; Tse, J. S.; Ratcliffe, C. I.; Leclerc, M. Highly Soluble Poly(2,7-carbazolenevinylene) for Thermoelectrical Applications: From Theory to Experiment. *React. Funct. Polym.* **2005**, *65*, 23−36.
(21) Hewitt, C. A.; Kaiser, A. B.; Roth, S.; Craps, M.; Czerw, R.; Carroll, D. L. Multilayered Carbon Nanotube/Polymer Composite Based Thermoelectric Fabrics. *Nano Lett.* **2012**, *12*, 1307−1310.
(22) Yu, C.; Kim, Y. S.; Kim, D.; Grunlan, J. C. Thermoelectric Behavior of Segregated-Network Polymer Nanocomposites. *Nano Lett.* **2008**, *8*, 4428−4432.
(23) Bounioux, C.; Diaz-Chao, P.; Campoy-Quiles, M.; Martin-Gonzalez, M. S.; Goni, A. R.; Yerushalmi-Rozene, R.; Muller, C. Thermoelectric Composites of Poly(3-hexylthiophene) and Carbon Nanotubes with a Large Power Factor. *Energy Environ. Sci.* **2013**, *6*, 918−925.
(24) He, M.; Qiu, F.; Lin, Z. Q. Towards High-Performance Polymer-Based Thermoelectric Materials. *Energy Environ. Sci.* **2013**, *6*, 1352−1361.
(25) Wang, Y. Y.; Cai, K. F.; Yao, X. Facile Fabrication and Thermoelectric Properties of PbTe-Modified Poly(3,4-ethylenedioxythiophene) Nanotubes. *ACS Appl. Mater. Interfaces* **2011**, *3*, 1163−1166.
(26) Du, Y.; Shen, S. Z.; Yang, W. D.; Cai, K. F.; Casey, P. S. Preparation and Characterization of Multiwalled Carbon Nanotube/poly(3-hexylthiophene) Thermoelectric Composite Materials. *Synth. Met.* **2012**, *162*, 375−380.
(27) Wang, Y. Y.; Cai, K. F.; Yao, X. One-Pot Fabrication and Enhanced Thermoelectric Properties of Poly(3,4-ethylenedioxythiophene)-Bi_2S_3 Nanocomposites. *J. Nanopart. Res.* **2012**, *14*, 848.
(28) Du, Y.; Shen, S. Z.; Yang, W. D.; Donelson, R.; Cai, K. F.; Casey, P. S. Simultaneous Increase in Conductivity and Seebeck Coefficient in a Polyaniline/Graphene Nanosheets Thermoelectric Nanocomposite. *Synth. Met.* **2012**, *161*, 2688−2692.
(29) See, K. C.; Feser, J. P.; Chen, C. E.; Majumdar, A.; Urban, J. J.; Segalman, R. A. Water-Processable Polymer−Nanocrystal Hybrids for Thermoelectrics. *Nano Lett.* **2010**, *10*, 4664−4667.
(30) Yang, J. H; Yip, H. L.; Jen, A. K. Y. Rational Design of Advanced Thermoelectric Materials. *Adv. Energy Mater.* **2013**, *3*, 549−565.
(31) Bubnova, O.; Khan, Z. U.; Malti, A.; Braun, S.; Fahlman, M.; Berggren, M.; Crispin, X. Optimization of the Thermoelectric Figure of Merit in the Conducting Polymer Poly(3,4-ethylenedioxythiophene). *Nat. Mater.* **2011**, *10*, 429−433.
(32) Kim, G. H.; Shao, L.; Zhang, K.; Pipe, K. P. Engineered Doping of Organic Semiconductors for Enhanced Thermoelectric Efficiency. *Nat. Mater.* **2013**, *12*, 719−723.
(33) Majumdar, A. Thermoelectricity in Semiconductor Nanostructures. *Science* **2004**, *303*, 777−778.
(34) Yan, H.; Ohta, T.; Toshima, N. Stretched Polyaniline Films Doped by (±)-10-Camphorsulfonic Acid: Anisotropy and Improvement of Thermoelectric Properties. *Macromol. Mater. Eng.* **2001**, *286*, 139−142.
(35) Sun, Y. M.; Wei, Z. M.; Xu, W.; Zhu, D. B. A Three-in-One Improvement in Thermoelectric Properties of Polyaniline Brought by Nanostructures. *Synth. Met.* **2010**, *160*, 2371−2376.
(36) Yakuphanoglu, F.; Senkal, B. F.; Sarac, A. Electrical Conductivity, Thermoelectric Power, and Optical Properties of Organo-Soluble Polyaniline Organic Semiconductor. *J. Electron. Mater.* **2008**, *37*, 930−934.
(37) Sun, J.; Yeh, M. L.; Jung, B. J.; Zhang, B.; Feser, J.; Majumdar, A.; Katz, H. E. Simultaneous Increase in Seebeck Coefficient and Conductivity in a Doped Poly(alkylthiophene) Blend with Defined Density of States. *Macromolecules* **2010**, *43*, 2897−2903.
(38) Zhao, X. B.; Hu, S. H.; Zhao, M. J.; Zhu, T. J. Thermoelectric Properties of $Bi_{0.5}Sb_{1.5}Te_3$/Polyaniline Hybrids Prepared by Mechanical Blending. *Mater. Lett.* **2002**, *52*, 147−149.
(39) Li, Y.; Zhao, Q.; Wang, Y. G.; Bi, K. Synthesis and Characterization of Bi_2Te_3/Polyaniline Composites. *Mater. Sci. Semicond. Process.* **2011**, *14*, 219−222.
(40) Toshima, N.; Imai, M.; Ichikawa, S. Organic−Inorganic Nanohybrids as Novel Thermoelectric Materials: Hybrids of Polyaniline and Bismuth(III) Telluride Nanoparticles. *J. Electron. Mater.* **2011**, *40*, 898−902.
(41) Wu, C. G.; DeGroot, D. C.; Marcy, H. O.; Schindler, J. L.; Kannewurf, C. R.; Liu, Y. J.; Hirpo, W.; Kanatzidis, M. G. Redox Intercalative Polymerization of Aniline in V2O5 Xerogel. The Postintercalative Intralamellar Polymer Growth in Polyaniline/Metal Oxide Nanocomposites Is Facilitated by Molecular Oxygen. *Chem. Mater.* **1996**, *8*, 1992−2004.
(42) Song, H. J.; Liu, C. C.; Zhu, H. F.; Kong, F. F.; Lu, B. Y.; Xu, J. K.; Wang, J. M.; Zhao, F. Improved Thermoelectric Performance of Free-Standing PEDOT:PSS/Bi_2Te_3 Films with Low Thermal Conductivity. *J. Electron. Mater.* **2013**, *42*, 1268−1274.
(43) Ren, L.; Qi, X.; Liu, Y. D.; Hao, G. L.; Huang, Z. Y.; Zou, X. H.; Yang, L. W.; Li, J.; Zhong, J. X. Large-Scale Production of Ultrathin Topological Insulator Bismuth Telluride Nanosheets by a Hydrothermal Intercalation and Exfoliation Route. *J. Mater. Chem.* **2012**, *22*, 4921−4926.
(44) Park, T.; Park, C.; Kim, B.; Shin, H.; Kim, E. Flexible PEDOT Electrodes with Large Thermoelectric Power Factors to Generate

Electricity by the Touch of Fingertips. *Energy Environ. Sci.* **2013**, *6*, 788−792.
(45) Taggart, D. K.; Yang, Y. A.; Kung, S. C.; McIntire, T. M.; Penner, R. M. Enhanced Thermoelectric Metrics in Ultra-Long Electrodeposited PEDOT Nanowires. *Nano Lett.* **2011**, *11*, 125−131.
(46) Mehta, R. J.; Zhang, Y. L.; Karthik, C.; Singh, B.; Siegel, R. W.; Borca-Tasciuc, T.; Ramanath, G. A New Class of Doped Nanobulk High-Figure-Of Merit Thermoelectrics by Scalable Bottom-up Assembly. *Nat. Mater.* **2012**, *11*, 233−240.
(47) Du, Y.; Cai, K. F.; Li, H.; An, B. J. The Influence of Sintering Temperature on the Microstructure and Thermoelectric Properties of *n*-Type $Bi_2Te_{3-x}Se_x$ Nanomaterials. *J. Electron. Mater.* **2011**, *40*, 518−522.
(48) Tritt, T. M. Thermoelectric Phenomena, Materials, and Applications. *Annu. Rev. Mater. Res.* **2011**, *41*, 433−448.
(49) Chatterjee, K.; Mitra, M.; Kargupta, K.; Ganguly, S.; Banerjee, D. Synthesis, Characterization and Enhanced Thermoelectric Performance of Structurally Ordered Cable-like Novel Polyaniline−Bismuth Telluride Nanocomposite. *Nanotechnology* **2013**, *24*, 215703.
(50) Zhang, B.; Sun, J.; Katz, H. E.; Fang, F.; Opila, R. L. Promising Thermoelectric Properties of Commercial PEDOT:PSS Materials and Their Bi_2Te_3 Powder Composites. *ACS Appl. Mater. Interfaces* **2010**, *2*, 3170−3178.
(51) Kim, D.; Kim, Y.; Choi, K.; Grunlan, J. C.; Yu, C. H. Improved Thermoelectric Behavior of Nanotube-Filled Polymer Composites with Poly(3,4-ethylenedioxythiophene) Poly(styrenesulfonate). *ACS Nano* **2010**, *4*, 513−523.
(52) Dresselhaus, M. S.; Chen, G.; Tang, M. Y.; Yang, R. G.; Lee, H.; Wang, D. Z.; Ren, Z. F.; Fleurial, J. P.; Gogna, P. New Directions for Low-Dimensional Thermoelectric Materials. *Adv. Mater.* **2007**, *19*, 1043−1053.
(53) Tsai, T. C.; Chang, H. C.; Chen, C. H.; Whang, W. T. Widely Variable Seebeck Coefficient and Enhanced Thermoelectric Power of PEDOT:PSS Films by Blending Thermal Decomposable Ammonium Formate. *Org. Electron.* **2011**, *12*, 2159−2164.
(54) Meng, C. Z.; Liu, C. H.; Fan, S. S. A Promising Approach to Enhanced Thermoelectric Properties Using Carbon Nanotube Networks. *Adv. Mater.* **2010**, *22*, 535−539.
(55) Martin-Gonzalez, M.; Caballero-Calero, O.; Diaz-Chao, P. Nanoengineering Thermoelectrics for 21st Century: Energy Harvesting and Other Trends in the Field. *Renewable Sustainable Energy Rev.* **2013**, *24*, 288−305.
(56) Fleurial, J. P.; Gailliard, L.; Triboulet, R.; Scherrer, H.; Scherrer, S. Thermal Properties of High Quality Single Crystals of Bismuth Telluride - Part I: Experimental Characterization. *J. Phys. Chem. Solids* **1988**, *49*, 1237−1247.
(57) Jiang, F. X.; Xu, J. K.; Lu, B. Y.; Xie, Y.; Huang, R. J.; Li, L. F. Thermoelectric Performance of Poly(3,4-ethylenedioxythiophene):Poly(styrenesulfonate). *Chin. Phys. Lett.* **2008**, *25*, 2202−2205.
(58) Scholdt, M.; Do, H.; Lang, J.; Gall, A.; Colsmann, A.; Lemmer, U.; Koenig, J. D.; Winkler, M.; Boettner, H. Organic Semiconductors for Thermoelectric Applications. *J. Electron. Mater.* **2010**, *39*, 1589−1592.
(59) Yu, C.; Choi, K.; Yin, L.; Grunlan, J. C. Light-Weight Flexible Carbon Nanotube Based Organic Composites with Large Thermoelectric Power Factors. *ACS Nano* **2011**, *5*, 7885−7892.
(60) Coates, N. E.; Yee, S. K.; McCulloch, B.; See, K. C.; Majumdar, A.; Segalman, R. A.; Urban, J. J. Effect of Interfacial Properties on Polymer-Nanocrystal Thermoelectric Transport. *Adv. Mater.* **2013**, *25*, 1629−1633.